Motional Heterogeneities in Siloxane/Poly(ethylene glycol) Ormolyte Nanocomposites Studied by ^{13}C Solid-State Exchange NMR

E. R. deAzevedo,[†] D. Reichert,[‡] E. L. G. Vidoto,[†] K. Dahmouche,[§] P. Judeinstein,[||] and T. J. Bonagamba*,[†]

Instituto de Física de São Carlos, Universidade de São Paulo, Caixa Postal 369, CEP: 13560-970, São Carlos, São Paulo, Brazil, Martin-Luther Universitaet Halle-Wittenberg, FB Physik, Friedemann-Bach-Platz 6, 06108 Halle/Saale, Germany, Instituto de Química de Araraquara - UNESP, Av. Prof. Francisco Degni s/n, CEP: 14800-900, Araraquara, São Paulo, Brazil, and Laboratoire de Chimie Structurale Organique, UPRESA, CNRS 8074, Université Paris-Sud, 91405 Orsay, France

Received September 20, 2002. Revised Manuscript Received March 14, 2003

^{13}C exchange solid-state NMR methods were used to study two families of siloxane/poly(ethylene glycol) hybrid materials: Types I and II, where the polymer chains interact with the inorganic phase through physical (hydrogen bonds or van der Waals forces) or chemical (covalent bonds) interactions, respectively. These methods were employed to analyze the effects of the interactions between the organic and inorganic phases on the polymer dynamics in the milliseconds to seconds time scale, which occurs at temperatures below the motional narrowing of the NMR line width and around the polymer glass transition. Motional heterogeneities associated with these interactions and evidence of both small and large amplitude motions were directly observed for both types of hybrids. The results revealed that the hindrance to the slow molecular motions of the polymer chains due to the siloxane structures depends on the chain length and the nature of the interaction between the organic and inorganic phases.

Introduction

The combination of the appropriate processing conditions with the adequate choice of organic and inorganic components dictates the morphology, molecular structure, and features of hybrid materials. The intense activity in this domain of research is due to the extraordinary implications that derive from the possibility of tailoring multifunctional advanced compounds by mixing, at the nanosize level, in a single material, organic and inorganic components. The hybrid concept seems to be particularly well-adapted for the production of advanced materials presenting ion-conducting properties with the advantage of replacing viscous liquid systems by solid or rubbery materials. However, these materials are used not only as solid polymer electrolytes (SPE)[1] but also as matrixes to entrap molecules with optical properties (fluorescence, photochromism, and nonlinear optic dyes)[2] or as thin films (protective layers).[3] In the case of SPE, lithium perchlorate is dissolved inside the matrixes, leading to materials with reasonable ionic conductivity (10^{-6}−10^{-4} S/cm) and the possibility of designing sol−gel-processed devices.[4]

Among the various systems that have been proposed in recent years, the family of versatile compounds, classified as di-ureasils, in which polyether-based chains are grafted on both ends to a siliceous backbone through urea functionalities is noteworthy.[5−7] When doped with Li salts, these solid, transparent, and flexible nanocomposites exhibit good ionic conductivity at room temperature ($\sim 10^{-6}$ S/cm). Due to the presence of covalent bonds between the inorganic and organic phases, these hybrids (Type II) have a higher chemical stability and better mechanical properties than siloxane-free polymer electrolytes. Siloxane−polyether nanocomposites presenting only physical bonds between the inorganic and organic phases (Type I) have also been obtained.[5,7,8] These rubbery blends have a higher room-temperature ionic conductivity ($\sim 10^{-4}$ S/cm) than the Type II hybrids but a much lower chemical stability.

In previous NMR studies,[5,7,9,10] large differences in the polymer dynamics for Types I and II materials were

* To whom correspondence should be addressed. E-mail: tito@if.sc.usp.br.
[†] Universidade de São Paulo.
[‡] Martin-Luther Universitaet Halle-Wittenberg.
[§] Instituto de Química de Araraquara - UNESP.
[||] Université Paris-Sud.

(1) Gray, F. M. *Polymer Electrolytes*; RSC Materials Monographs; Royal Society of Chemistry: Cambridge, 1997.
(2) Chaumel, F.; Jiang, H.; Kakkar, A. *Chem. Mater.* **2001**, *13*, 3389−3395.
(3) Mitzi, D. B. *Chem. Mater.* **2001**, *13*, 3283−3298.
(4) Štangar, U. L.; Orel, B.; Grošelj, N.; Judeinstein, P.; Decker, F.; Lianos, P. *Monatsh. Chem.* **2001**, *132*, 103−112.
(5) Judeinstein, P.; Brik, M. E.; Bayle, J. P.; Courtieu, J.; Rault, J. *Mater. Res. Soc. Symp. Proc.* **1994**, *346*, 937−942.
(6) Ravaine, D.; Seminel, A.; Charbouillot, Y.; Vincens, M. *J. Non-Cryst. Solids* **1986**, *82*, 210−219.
(7) Brik, M. E.; Titman, J. J.; Bayle, J. P.; Judeinstein, P. *J. Polym. Sci., Part B: Polym. Phys.* **1996**, *34*, 2533−2542.
(8) Lesot, P.; Chapuis, S.; Bayle, J. P.; Rault, J.; Lafontaine, E.; Campero, A.; Judeinstein, P. *J. Mater. Chem.* **1998**, *8*, 147−151.
(9) Mello, N. C.; Bonagamba, T. J.; Panepucci, H.; Dahmouche, K.; Judeinstein, P.; Aegerter, M. A. *Macromolecules* **2000**, *33*, 1280−1288.
(10) de Souza, P. H.; Bianchi, R. F.; Dahmouche, K.; Judeinstein, P.; Faria, R. M.; Bonagamba, T. J. *Chem. Mater.* **2001**, *13*, 3685−3692.

10.1021/cm020947v CCC: $25.00
Published on Web 04/25/2003

observed. These differences were related to the following ormolyte compositional parameters: the weight percent of polymer, the polymerization degree, the nature of the interface between organic and inorganic phases, and the lithium doping levels. Because the segmental mobility of the polymer chain promotes ion motion and diffusion, these differences also induce variations in the ion mobility and, consequently, in the ionic conductivity.[11] Therefore, understanding the polymer dynamics within the inorganic matrix is crucial for understanding the ion conductivity of the ormolytes. Additionally, the knowledge of segmental motion is also important for mechanical and adhesive properties.[12]

At room temperature, well above the polymer glass transition, it was already observed for Type II nanocomposite[7] that the segmental mobility is not uniform along the polymer chain. Using electron paramagnetic resonance measurements to analyze samples prepared with nitroxide spin probes, motional heterogeneities were observed and associated with the motional hindrance due to covalent bonds. These results were corroborated by NMR rotating-frame relaxation time ($T_{1\rho}$) measurements. However, no information about the motional amplitudes, which can also reflect motional heterogeneities, were taken from these studies because the employed techniques are not very sensitive to these parameters.

This work reports a ^{13}C solid-state exchange NMR study of nondoped hybrids based on SiO_2−poly(ethylene glycol) networks to obtain detailed information about the time scale, amplitude, and heterogeneities of slow molecular motions in the hybrid organic phase. Since the applicability of the NMR exchange methods is restricted to the study of motions with correlation times ranging from milliseconds to seconds, the experiments were performed at temperatures below the motional narrowing of the ^{13}C NMR spectra and around the polymer glass transition. At these temperatures, the molecular motion is much slower than that at room temperature where the ion conductivity is normally of interest. However, the exchange experiments yield additional information about the segmental mobility and it is worthwhile to perform them because many of the results can be extended to room temperature.

NMR Background

This section gives a short introduction about the exchange methods employed in this work. Detailed descriptions of the methods described below are found in refs 13−19.

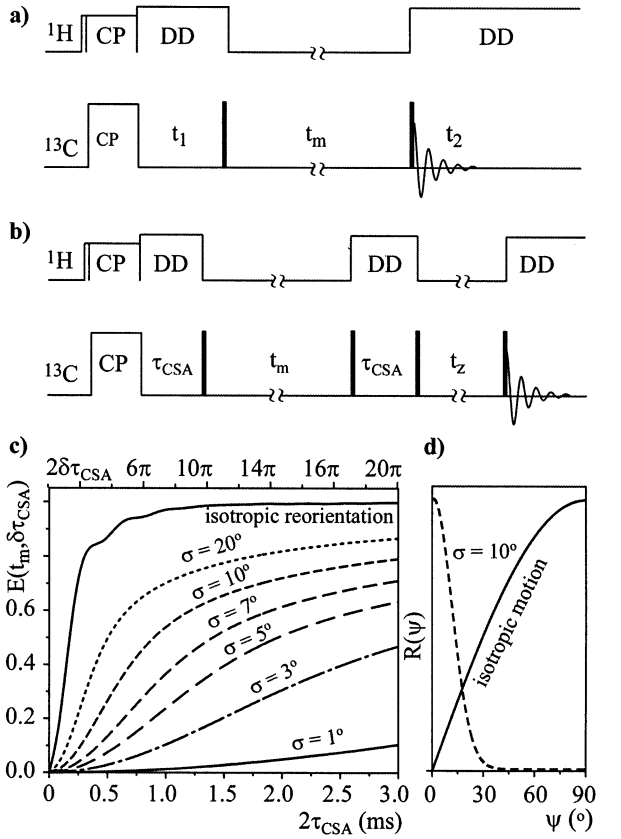

Figure 1. Pulse sequence used in the exchange experiments and simulations of 1D PUREX curves as a function of $2\tau_{CSA}$. (a) 2D exchange pulse sequence. (b) 1D PUREX pulse sequence. (90° pulses are filled black.) (c) $E(t_m,\delta\tau_{CSA})$ vs $2\tau_{CSA}$ curves for rotations around the C−C bond in PEG chains. A distribution of reorientation angles is considered by weighing the curves for individual rotation angles using a Gaussian function and then adding the results to produce $E(t_m,\delta\tau_{CSA})$ vs $2\tau_{CSA}$. The root-mean-square (rms) widths (σ) of the Gaussians are indicated. The obtained curve for fully isotropic reorientations is also shown. (d) Typical reorientation angle distributions for small-angle rotation ($\sigma = 10°$) and isotropic motion are presented. In the case of isotropic motion the rotation angle (ψ) is equal to the reorientation angle (β_R).

Exchange NMR experiments provide the most specific information about slow motions ($\tau_c \sim$ ms−s) in organic materials. Using these techniques, details of slow molecular reorientations, such as amplitude and time scale, can be directly probed. For this reason, it is worthwhile to apply solid-state NMR exchange methods to investigate the polymer dynamics, making possible the study of local[20,21] or segmental motions[22] responsible for the dynamic processes in these materials.

2D Exchange NMR. Figure 1a shows the pulse sequence for the static 2D exchange experiment. In this experiment the orientation-dependent NMR frequencies are monitored before (t_1) and after (t_2), a mixing time (t_m) when molecular reorientations can occur. If no exchange happens, the resulting 2D spectrum is purely diagonal. In contrast, if slow molecular reorientations

(11) Judeinstein, P.; Titman, J.; Stamm, M.; Schmidt, H. *Chem. Mater.* **1994**, *6*, 127−134.
(12) Mark, J. E. *Solid State & Materials Science* **1999**, *4*, 565−570.
(13) deAzevedo, E. R.; Bonagamba, T. J.; Schmidt-Rohr, K. *J. Magn. Reson.* **2000**, *142*, 86−96.
(14) deAzevedo, E. R.; Hu, W.-H.; Bonagamba, T. J.; Schmidt-Rohr, K. *J. Chem. Phys.* **2000**, *112*, 8988−9001.
(15) Jeener, J.; Meier, B. H.; Bachmann, P.; Ernst, R. R. *J. Chem. Phys.* **1979**, *71*, 4546−4553.
(16) Wefing, S.; Spiess, H. W. *J. Chem. Phys.* **1988**, *89*, 1219−1233.
(17) Wefing, S.; Kaufmann, S.; Spiess, H. W. *J. Chem. Phys.* **1988**, *89*, 1234−1244.
(18) Kaufmann, S.; Wefing, S.; Schaefer, D.; Spiess, W. *J. Chem. Phys.* **1990**, *1*, 197−214.
(19) Schmidt-Rohr, K.; Spiess, H. W. *Multidimensional Solid-State NMR and Polymers*, 1st ed.; Academic Press: London, 1994; Vol. 1.
(20) Reichert, D.; Hempel, G.; Zimmermann, H.; Tekely, P.; Poupko, R.; Luz, Z.; Favre, D. E.; Chmelka, B. F. *Appl. Magn. Reson.* **1999**, *17*, 315−327.
(21) Schmidt-Rohr, K.; Kulik, A. S.; Beckham, H. W.; Ohlemacher, A.; Pwelzik, U.; Spiess, H. W. *Macromolecules* **1994**, *27*, 4733−4745.
(22) Schaefer, D.; Spiess, H. W.; Suter, U. W.; Fleming, W. W. *Macromolecules* **1990**, *23*, 3431−3439.

occur during t_m, off-diagonal intensities are observed. The shape of the 2D spectrum strongly depends on motional amplitude, making it possible to distinguish whether the motion involves small (<20°) or large amplitude reorientations. The identification of the motional amplitude can be made directly from the 2D spectrum without the need of any specific model. This makes the 2D exchange method particularly powerful in this work, where the main interest is to discuss the differences between the motional behavior according to the composition and the nature of the cross-links in ormolytes samples. Furthermore, the 2D exchange spectrum also provides more specific information about the geometry of the slow motion because it allows distinguishing between discrete jumps and diffusive motions.

1D Pure Exchange (PUREX) Method. The pulse sequence for the 1D PUREX NMR experiment is shown in Figure 1b. Simply put, 1D PUREX is a stimulated-echo[23] experiment with suppression of the nonmobile segments in the milliseconds to seconds time scale. The principle of the experiment is briefly summarized here. A more detailed discussion about PUREX can be found in ref 13. Basically, the experiment detects the signal reduction resulting from changes in the orientation-dependent chemical-shift frequencies that occur due to segmental reorientations during the mixing time t_m. During the first evolution period, τ_{CSA}, the spins evolve under the chemical-shift anisotropy (CSA), which is represented by the anisotropy parameter $\delta = \sigma_{ZZ} + \sigma_{iso}$.[24] Then, the magnetization is stored along the z-direction so that it does not precess or dephase during the mixing time. If no motions occurred during t_m, the chemical-shift evolution, after a read-out pulse and another evolution period under chemical-shift anisotropy (total time of $2\tau_{CSA}$), is refocused at the end of the second τ_{CSA} period. At this point the magnetization is stored again along the z-direction during a short period $t_z \ll \tau_C$ and then flipped back to the transverse plane for detection. If segmental reorientation occurred during t_m, the orientation-dependent frequency has changed and the chemical-shift anisotropy is not completely refocused. The resulting dephasing is observed as a decrease in the detected line intensity. To remove T_1- and T_2-relaxation effects during t_m and $2\tau_{CSA}$, respectively, a reference spectrum $S_0 = S(t_m = t_z,\delta\tau_{CSA})$, which has the same relaxation factors but negligible motion effects during t_m, is measured. It is obtained by simply swapping t_m and t_z. To remove the contribution of nonmobile segments in the milliseconds to seconds time scale, the 1D PUREX intensity $S = S(t_m,\delta\tau_{CSA})$ is subtracted from the reference spectrum S_0. Dividing this difference by S_0, one can obtain a normalized pure-exchange intensity $E(t_m,\delta\tau_{CSA}) = \Delta S/S_0$, which does not contain contributions from rigid segments and relaxation effects.

The t_m dependence of $E(t_m,\delta\tau_{CSA})$ yields the time scale of the slow motions occurred during t_m, while the τ_{CSA} dependence of $E(t_m,\delta\tau_{CSA})$ provides the motional amplitude. The smaller the reorientation angles, the slower the increase of the $E(t_m,\delta\tau_{CSA})$ as a function of τ_{CSA}. This is demonstrated in Figure 1c, where simulated curves for rotations around the C−C bond in PEG chains are provided. It must be pointed out that $E(t_m,\delta\tau_{CSA})$ versus $2\tau_{CSA}$ curves are very sensitive to the motional amplitude, but not to the motional geometry. In other words, it is difficult to distinguish motions occurring around different axes only by analyzing the $E(t_m,\delta\tau_{CSA})$ versus $2\tau_{CSA}$ build-up curves, but it is easy to discriminate motions occurring with distinct amplitudes, mainly for small-angle motions, Figure 1c. Thus, these rotations around the C−C bonds can be used as an approximation to estimate the amplitude of small-angle rotations in PEG chains.

If the molecular motion occurs following a distribution of reorientation angles, $R(\beta_R,t_m/\tau_C)$, the $E(t_m,\delta\tau_{CSA})$ versus $2\tau_{CSA}$ curves are simply a $R(\beta_R,t_m/\tau_C)$-weighted superposition of 1D PUREX curves for each specific reorientation angle, β_R, $\epsilon(t_m,\delta\tau_{CSA})$, that is,

$$E(t_m,\delta\tau_{CSA}) = \int_0^{90°} R(\beta_R,t_m/\tau_C)\epsilon(t_m,\delta\tau_{CSA})\, d\beta_R \quad (1)$$

In amorphous PEG chains a single reorientation angle is not expected. Consequently, the curves shown in Figure 1c are calculated considering a Gaussian distribution of reorientation angles with root-mean-square, σ, given in Figure 1c; that is, a restricted diffusive rotation is assumed. The curves reveal good resolution for small rotation angles (σ < 20°), which can be explained by analysis in terms of the CSA difference tensor.[14] Figure 1c also shows the $E(t_m,\delta\tau_{CSA})$ versus $2\tau_{CSA}$ curves for fully isotropic rotations. Figure 1d shows the reorientation angle distributions for both models, $R(\psi)$. Due to this high sensitivity to small-angle reorientations, it is advantageous to use 1D PUREX to complement the information about the motional amplitude taken from the 2D exchange experiment.

Materials and Methods

Sample Preparation. The synthesis of Type I[25,26] and Type II[5,7,8] hybrid materials based on SiO_2 and poly(ethylene glycol)−$HO(CH_2CH_2O)_nH$ (PEG)−with various molecular weights were already detailed elsewhere. In Type I, only weak interactions are expected to link together the organic and inorganic components while in Type II chemical bonds of urea type are formed between the two phases. Therefore, in Type II ormolytes the polymer chain has the following chemical structure: $\{_{3/2}OSi(CH_2)_3NHCONH(CH_2)_3[OCH_2CH_2]_nO(CH_2)_3NHCONH(CH_2)_3SiO_{3/2}\}_p$. After the preparation and further drying to remove the solvents (vacuum heating), the nanocomposites were immediately sealed in appropriate glass tubes for NMR experiments.

The following nomenclature will be used to describe the composites: $[X]_n$-Z, where X represents the weight percent of the polymer, n the polymerization degree, and Z equals I or II, for the corresponding type of ormolyte, nonbonded and chemically bonded, respectively.

To understand the effects of polymer chain length and the nature of the silica−polymer interface (physical or chemical bonds) on the polymer dynamics, the following set of samples was prepared: $[50]_{14}$-I, $[50]_{45}$-I, $[66]_{11}$-II, and $[88]_{45}$-II. The

(23) Fujara, F.; Welfing, S.; Spiess, W. H. *J. Chem. Phys.* **1986**, *84*, 4579−4584.
(24) Veeman, W. S. *Prog. Nucl. Magn. Reson. Spectrosc.* **1984**, *16*, 193−235.
(25) Dahmouche, K.; Atik, M.; Mello, N. C.; Bonagamba, T. J.; Panepucci, H.; Aegerter, M.; Judeinstein, P. *Mater. Res. Soc. Symp. Proc.* **1996**, *435*, 363−368.
(26) Dahmouche, K.; Atik, M.; Mello, N. C.; Bonagamba, T. J.; Panepucci, H.; Aegerter, M. A.; Judeinstein, P. *J. Sol.-Gel Sci. Technol.* **1997**, *8*, 711−715.

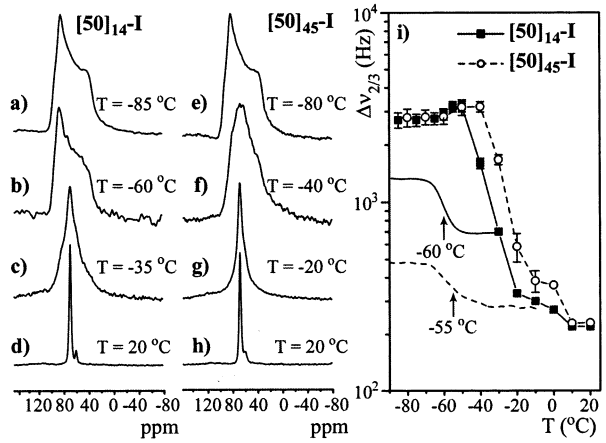

Figure 2. ^{13}C line shape analysis of Type I ormolytes around their glass transition temperatures. ^{13}C direct-polarization spectra as a function of the temperature for the samples $[50]_{14}$-I (a−d) and $[50]_{45}$-I (e−h). (i) Line width at $^2/_3$ of the maximum intensity measured as a function of temperature for both hybrids. The small broadenings observed in the line widths around $T = -10$ °C are due to the maximization of the ^{13}C spin−lattice relaxation rate ($\Delta\nu \approx T_1^{-1}$. For comparison, the solid and dashed lines represent the DSC curves for $[50]_{14}$-I and $[50]_{45}$-I samples, respectively, with arbitrary units along the *y* axis.

nonbonded samples were prepared with the same weight percent of polymer and different degrees of polymerization to analyze the effects of the polymer chain length on the polymer dynamics. The same procedure was used to prepare the bonded samples; however, in this case *n* and *X* are codependent parameters. Due to this reason and with the purpose of comparing the polymer dynamics in both types of nanocomposites, Type I and Type II hybrids were prepared with the choice of PEG with polymerization degree as similar as possible.

Differential Scanning Calorimetry (DSC). DSC measurements were performed with a scan rate of 10 °C/min from −100 to 0 °C using Texas Instruments model 2910 equipment.

NMR. The experiments were performed using a 9.4 T−VARIAN INOVA spectrometer at ^{13}C and ^1H frequencies of 100.5 and 400.0 MHz, respectively. A 7-mm static double-resonance variable temperature Doty probe head was used. $\pi/2$ pulse lengths of 3.8 and 4.5 μs were applied for ^{13}C and ^1H, respectively. The proton decoupling field strength of approximately 65 kHz, cross-polarization time of 1.5 ms, and recycle delays ranging from 10 to 30 s were used. In 2D exchange experiments 64−128 increments in t_1 were acquired using a total of 32 scans per t_1 point. The mixing times for 2D experiments were 200 ms. Hypercomplex acquisition was used to achieve a pure-absorptive 2D spectrum.[27] The 1D pure exchange NMR (1D PUREX) experiments were performed using mixing times ranging form 0.1 to 1.0 s and τ_{CSA} values ranging from 20 to 1500 μs.

Results and Discussion

Line Shape Analysis. Complementary to the exchange techniques, the temperature dependence of the ^{13}C line shape can give information about the polymer dynamics in the microseconds to milliseconds time scale, due to the orientation dependence of the chemical shift anisotropy (CSA). Parts (a)−(d) and (e)−(h) of Figure 2 show the line shape temperature dependence for both nonbonded ormolytes. The spectra obtained at 20 °C show two distinguishable isotropic lines at 58 and 67 ppm. The line at 58 ppm is attributed to the CH_2 groups nearby the OH terminal groups of PEG, while the main line at 67 ppm is the typical signal of the $[CH_2CH_2O]_n$ groups. In the rigid-lattice regime, at the lowest temperatures, a typical PEG powder pattern is observed ($\sigma_{xx} = 93$ ppm, $\sigma_{yy} = 82$ ppm, and $\sigma_{zz} = 33$ ppm),[28,29] parts (a) and (e) of Figure 2 for samples $[50]_{14}$-I and $[50]_{45}$-I, respectively. As the temperature increases, the molecular motion starts averaging the CSA interaction, producing a distortion in the powder spectrum, Figure 2b,f. This distortion increases until featureless broad lines are obtained, Figure 2c,g. At higher temperatures the motional rate, $k \approx (\tau_c)^{-1}$, becomes larger than the full width of CSA, $\Delta\sigma = |\sigma_{xx} - \sigma_{zz}| = 60$ ppm ≈ 6 kHz, producing the complete averaging of this interaction and resulting in an isotropic line, Figure 2d,h. The motional narrowing is usually quantified by measuring the temperature dependence of the line width at half-maximum, $\Delta\nu_{1/2}$, or equivalently the full width of the CSA, $\Delta\sigma$. However, the powder pattern distortion occurring around the onset of the motional narrowing cannot be observed by measuring $\Delta\nu_{1/2}$ or $\Delta\sigma$ versus temperature. On the other hand, when the line width is taken at two-thirds of the maximum height, an initial broadening precedes the motional narrowing, which reflects the powder pattern distortion due to motions occurring with rates of a few KHz. Therefore, all the line widths were measured at two-thirds of the maximum height, $\Delta\nu_{2/3}$, because it provides a good indication of the temperature where the motional rates become smaller than kHz, facilitating the choice of the correct temperature for performing 2D exchange experiments. Figure 2i shows the temperature dependence of $\Delta\nu_{2/3}$ for both Type I samples together with the respective DSC traces shown with arbitrary units. Usually, the line width transitions observed for ormolytes are associated with the increase of the chain motion that occurs close to the polymer glass transition.[9] Similar results for the bonded samples are presented in Figure 3a−i. The spectral lines were already assigned in ref 7. The line (1) at 68 ppm is typical of $[CH_2CH_2O]_n$ groups in PEG chains. However, some extra lines show up in the NMR spectra of the sample $[66]_{11}$-II. The lines (2) and (3) are attributed to carbons in the linker group $[-Si(CH_2)_3NHCONH(CH_2)_3-]$. Line (4) is a signal from the probe background, which is present in all the spectra but not seen for several samples due to its relatively small amplitude. The spectra of the sample $[88]_{45}$-II also show lines (2) and (3), but due to the larger number of $[CH_2CH_2O]_n$ groups only one linkage carbon signal at 14 ppm (3) can be observed within the scale shown in Figure 3. With these identifications, the 20 to −20 ppm spectral region can be attributed to carbons in the linkage group. Thus, the right-side shoulder observed in the powder spectrum at low temperatures can be ascribed to these lines. This is an important feature because it will allow distinguishing the dynamic behavior of the segments near the linkage from the $[CH_2CH_2O]_n$ carbons. Another important feature of the spectra at 20 °C shown in Figures 2 and 3 concerns the fact that the ^{13}C lines of the $[CH_2CH_2O]_n$ groups are isotropic; that is, the molecular

(27) States, D. J.; Haberkorn, R. A.; Ruben, D. J. *J. Magn. Reson.* **1982**, *48*, 286−292.

(28) Harris, D. J.; Bonagamba, T. J.; Hong, M.; Schmidt-Rohr, K. *Macromolecules* **2000**, *33*, 3375−3381.

(29) Harris, D. J.; Bonagamba, T. J.; Hong, M.; Schmidt-Rohr, K. Submitted to *Polymer*, **2003**.

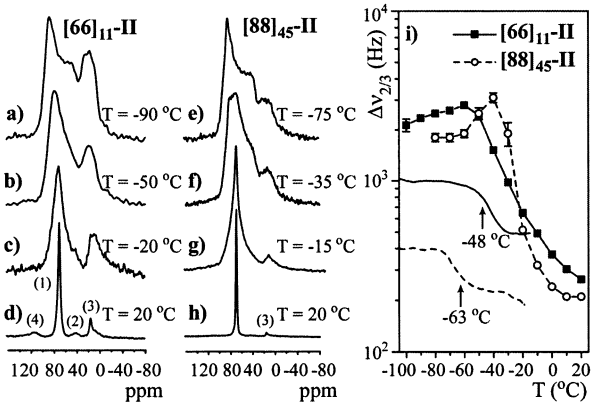

Figure 3. ^{13}C line shape analysis of Type II ormolytes around their glass transition temperatures. ^{13}C direct-polarization spectra as a function of the temperature for the samples $[66]_{11}$-II (a−d) and $[88]_{45}$-II (e−h). (i) Line width at $^2/_3$ of the maximum intensity measured as a function of temperature for both hybrids. For comparison, the solid and dashed lines represent the DSC curves for $[66]_{11}$-II and $[88]_{45}$-II samples, respectively, with arbitrary units along the *y*-axis.

motion completely averages the CSA anisotropy. Isotropic lines in the fast motion limit can result either from any kind of isotropic motions or from jumps between equivalent tetrahedral sites.[30,31] As the polymer interaction with the silica structure prevents the crystallization of the PEG chains (i.e., the polymer chains are expected to be fully amorphous), the presence of discrete jumps between tetrahedral sites are very unlikely for these systems. Therefore, the isotropic lines observed at 20 °C suggest the presence of isotropic molecular motion of the $[CH_2CH_2O]_n$ groups.

Simulation of the ^{13}C line shapes versus temperature could bring information about molecular motion in the microseconds to milliseconds time scale. However, it has not been done because in the case of heterogeneous systems such as ormolytes a large distribution of motional rates and complex motional geometries make it difficult to perform this calculation and extract motional parameters. Clear information is obtained from exchange experiments where slow molecular reorientations in the milliseconds to seconds time scale are observed. Therefore, the line-narrowing process was analyzed only to obtain the temperatures where these exchange experiments must be carried out.

Exchange experiments are sensitive to motions in the milliseconds to seconds time scale. Consequently, the temperatures must be chosen in such a way that most of the molecular segments move within this time scale. This slow motion regime can be selected based on the information contained in Figures 2 and 3. As discussed above, in the transition from kHz to Hz motional rates the line shape changes from a distorted (intermediate temperature range) to a regular (low-temperature range) powder pattern. As a result, $\Delta\upsilon_{2/3}$ decreases until a constant value is reached. In this plateau the rate of the molecular motion is smaller than or equal to Hz. This occurs at temperatures up to −50, −45, −60, and −40 °C for the samples $[50]_{14}$-I, $[50]_{45}$-I, $[66]_{11}$-II, and $[88]_{45}$-II, respectively.

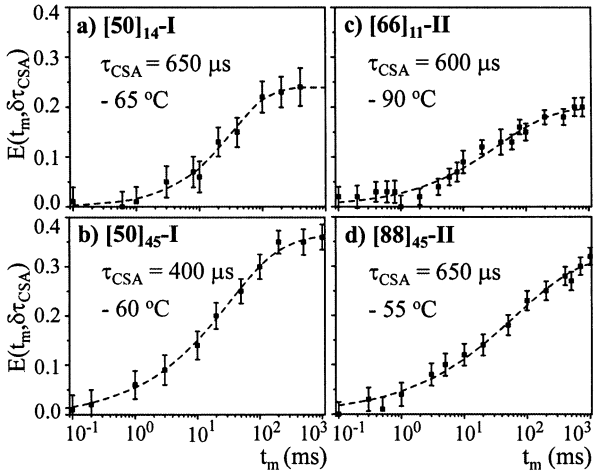

Figure 4. 1D PUREX intensities, $E(t_m,\delta\tau_{CSA})$, as a function of the mixing time. These experiments were performed with evolution times τ_{CSA} and temperatures as indicated in the figure. The curves were fitted using the KWW function. The mean correlation times and the β_{KWW} parameters obtained from the fittings were as follows. $[50]_{14}$-I: $\langle\tau_C\rangle = (40 \pm 10)$ ms and $\beta_{KWW} = 0.7 \pm 0.1$. $[50]_{45}$-I: $\langle\tau_C\rangle = (60 \pm 5)$ ms and $\beta_{KWW} = 0.55 \pm 0.04$. $[66]_{11}$-II: $\langle\tau_C\rangle = (70 \pm 10)$ ms and $\beta_{KWW} = 0.50 \pm 0.05$. $[80]_{45}$-II: $\langle\tau_C\rangle = (170 \pm 20)$ ms and $\beta_{KWW} = 0.45 \pm 0.04$.

Time Scale of the Slow Polymer Chain Motion. The time scale of the slow polymer chain motion was determined using 1D PUREX experiments. Figure 4 shows the 1D PUREX intensities, $E(t_m,\delta\tau_{CSA})$, as a function of the mixing time for the samples $[50]_{14}$-I, $[50]_{45}$-I, $[66]_{11}$-II, and $[88]_{45}$-II at −65, −60, −90, and −55 °C, respectively. The τ_{CSA} values used in the experiments were chosen in such a way that $\delta\tau_{CSA} > 2\pi$; that is, the dephasing due to the chemical shift anisotropy is complete. The spectral intensities used to calculate $E(t_m,\delta\tau_{CSA})$ were taken in the 70−100 ppm region so that they just account for the main line contribution, $[CH_2CH_2O]_n$, in the bonded ormolytes. For all hybrids nonexponential behavior of the $E(t_m,\delta\tau_{CSA})$ build-up curves was observed. This indicates that the slow motion occurs following a distribution of correlation times,[32] which is taken into account by fitting the curves by the Kohlrausch−Williams−Watt (KWW) function,[33] $f_m\{1 - \exp[(-t_m/\tau_0)^{\beta_{KWW}}]\}$, as shown in Figure 4. The β_{KWW} values and the calculated mean correlation times, $\langle t_C\rangle = (\tau_0/\beta_{KWW})\Gamma(1/\beta_{KWW})$, are shown in the caption of Figure 4. In the case of ormolytes, this distribution of correlation times can be associated with the hindrance in the motion of some polymer segments due to the polymer/siloxane interactions. However, no specific information about this interaction can be extracted because the presence of distributions of correlation times in the molecular motion of amorphous polymers near the glass transition is observed even for homopolymers and is generally attributed to the heterogeneous nature of these systems.[22,34,35] Actually, this could be obtained from a comparison with the slow motional rates around

(30) Spiess, H. W. In *NMR Basic Principles and Progress*; Springer-Verlag: New York, 1978; Vol. 15, p 55.
(31) Reichert, D.; Schneider, H. *Z. Phys. Chem.* **1995**, *190*, 63−71.
(32) Schmidt-Rohr, K.; Spiess, H. W. *Phys. Rev. Lett.* **1991**, *66*, 3020−3023.
(33) Williams, G.; Watts, D. C. *Trans. Faraday Soc.* **1970**, *66*, 80−85.
(34) McCrum, N. G.; Read, B. E.; Williams, G. *Anelastic and Dielectric Effects in Polymeric Solids*, 2nd ed.; Dover: New York, 1991; Vol. 1.
(35) Zemke, K.; Schmidt-Rohr, K.; Spiess, H. W. *Acta Polym.* **1994**, *45*, 148−159.

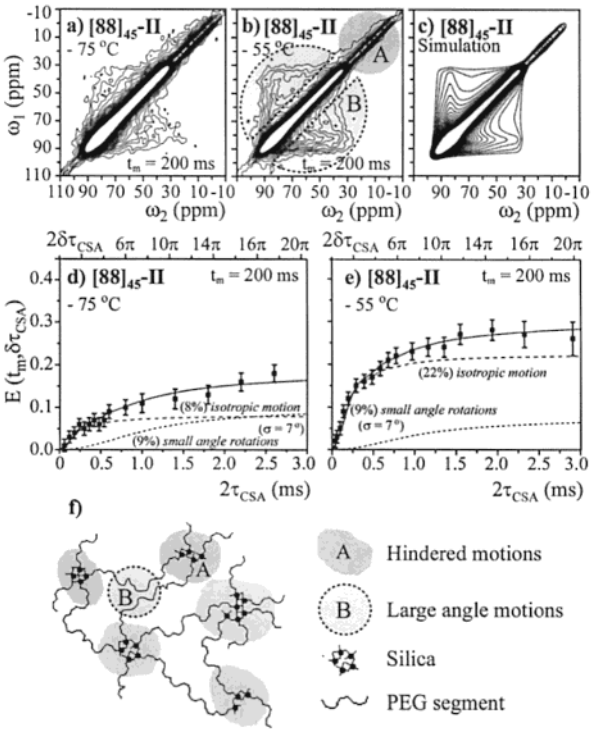

Figure 5. Results of exchange experiments performed for the $[80]_{45}$-II hybrid. (a) 2D exchange spectrum at −75 °C. (b) 2D exchange spectrum at −55 °C. The slowing down of the molecular motion is observed by the smaller number of contour lines in (a). (c) Simulation of the 2D exchange spectra based on the isotropic motion of about 30% of the polymer segments. This simulation was performed in the frequency domain, using the method discussed in refs 16 and 19. (d) Pure exchange intensity, $E(t_m,\delta\tau_{CSA})$ versus $2\tau_{CSA}$ at −75 °C. (e) Same as in (d) at −55 °C. The experimental curves were simulated by the superposition of small-angle rotations around the C−C bond, distributed as Gaussian functions, and fully isotropic reorientations. The percentage of each individual contribution and the rms width, σ, of the Gaussians are indicated in the figure. Reorientation angle distributions are shown in Figure 1. CSA tensor orientations and principal values from ref 37 were used. The contour levels were taken from 5 to 20% of the maximum height. (f) Schematic representation of the PEG chains showing the motional domains, regions A and B, associated with the different regions of the 2D exchange spectrum presented in Figure 5b.

the glass transition of the amorphous regions in neat PEG chains. However, neat PEG is highly crystalline and, consequently, it is very difficult to select only the amorphous regions to study the slow motions around the glass transition in this polymer, even when the PUREX technique is used. Moreover, in all physical mixtures that prevent crystallization of PEG, the fillers interact with the polymer chains, as in the case of Type I ormolytes. This makes it difficult to obtain detailed information about the polymer/siloxane interactions by just analyzing the slow motional rates and the analysis of motional amplitudes is useful.

Amplitude of the Polymer Chain Motion. The amplitude of the polymer chain motion was studied by both 2D exchange and 1D PUREX experiments. Parts (a) and (b) of Figure 5 show the observed 2D exchange spectra for the sample $[88]_{45}$-II at two different temperatures. The spectra were acquired with mixing times of 200 ms. The spectrum of the sample $[88]_{45}$-II at −55 °C (Figure 5b) clearly shows two distinct regions. In the spectral region ranging from −10 to 20 ppm, region A, the observed exchange pattern is fully diagonal, indicating that the molecular segments responsible for this component do not move in the milliseconds to seconds time scale. As discussed before, the signal in this region is attributed to the ^{13}C nuclei in the linkage group. On the other hand, from 20 to 95 ppm an exchange pattern composed by both diagonal and nondiagonal intensities (region B) is observed, indicating the presence of rigid and mobile segments performing large amplitude reorientations in the milliseconds to seconds time scale. Figure 5b shows a clear model free picture of the strong hindrance to the molecular motion due to the siloxane structure because it directly reveals the distinct dynamic behavior of segments near the siloxane structures. A pictorial representation of these chain motions is schematized in Figure 5f. No defined elliptical pattern is observed, indicating that the motion of the $[CH_2\text{-}CH_2O]_n$ groups does not involve defined jump angles, as in the case of helical jumps observed for crystalline poly(ethylene oxide) (PEO).[19] This is confirmed by the simulated spectrum shown in Figure 5c. This spectrum was calculated using a superposition of rigid (diagonal portion) and mobile segments undergoing isotropic reorientations, that is, for the reorientation angle distribution given in Figure 1d and using the procedure described in ref 19. Thus, the isotropic reorientations essentially show that most of these segments execute large angle motions as indicated in Figure 1d. The carbon signals from the linker were taken into consideration in the simulated spectrum using a diagonal Gaussian-shaped pattern centered at 15 ppm and with a width of 5 ppm. Furthermore, the diagonal pattern in the 20−95 ppm region indicates that the presence of silica structure hinders the molecular motions also in segments not located in the linkage. As a result, some of these molecular segments will execute small-angle reorientations while others will move slower than the milliseconds to seconds time scale, increasing the distribution of correlation times. It is important to notice that hindrance to the molecular motion results either in the slow down of the segment dynamics or in the decrease of the motional amplitude. Wefing, Kaufmann, and Spiess[17] have shown for isotropic rotational diffusion that, for a fixed mixing time, a decrease in the correlation time results directly in a reduction of the motional amplitude. Therefore, the occurrence of small-angle motion during the mixing time is also an indication that the segments performing these motions are slowed. To detect the possible small-angle reorientations, 1D PUREX versus $2\tau_{CSA}$ measurements were performed. As discussed previously, this technique is more sensitive to small-angle motions than the 2D exchange experiment, which makes it particularly useful in this context. The $E(t_m,\delta\tau_{CSA})$ versus τ_{CSA} curves for the sample $[88]_{45}$-II at −75 and −55 °C are shown in (d) and (e) of Figure 5. The spectral intensities S and S_0 were obtained by integrating the spectra from 70 to 100 ppm; that is, only the signal from $[CH_2CH_2O]_n$ groups were taken into consideration. Recently, it was demonstrated that the dipolar coupling to relaxing heteronuclei, such as ^{14}N, might also serve as an

exchange mechanism for the ^{13}C.[36] Therefore, taking only the contribution of the $[CH_2CH_2O]_n$ groups minimizes this effect because these carbons are at least 3 bonds far from ^{14}N present in the linker group.

The initial increase of the curve, for $2\delta\tau_{CSA} < 2\pi$, is associated with large-angle rotations. However, instead of reaching a constant value, the curve keeps increasing for $2\delta\tau_{CSA} > 2\pi$, which indicates that a percentage of the molecular segments undergo small-angle motion in the milliseconds to seconds time scale. The simulations shown in Figure 5d,e were based on the superposition of these two motional models. A good agreement between experimental and simulated data is obtained considering a superposition of isotropic rotations and restricted diffusion around the C−C bond with CSA tensors extracted from refs 28 and 29. As discussed previously, a good estimation of the motional amplitude can be made from the $E(t_m,\delta\tau_{CSA})$ versus $2\tau_{CSA}$ curves, but the motional geometry cannot be fully extracted from this experiment. In this sense, the use of restricted rotational diffusion around the C−C bond is just an approximation to consider these small-angle reorientations. Using this bimodal behavior for the segmental motions, the experimental curve can be fitted, suggesting that the hindrance to molecular motion imposed by the covalent bonds extends for segments not directly linked to the silica structure. Another interesting feature of the $E(t_m,\delta\tau_{CSA})$ versus $2\tau_{CSA}$ curve is the final value $E_\infty = E(t_m \gg \langle\tau_C\rangle, \delta\tau_{CSA} \gg 2\pi)$. As this value is proportional to the number of segments moving in the milliseconds to seconds time scale,[13] it can be seen that ~70% of the segments are moving out of this time scale at −55 °C, Figure 5e, which accounts for the diagonal observed in the 2D exchange spectrum. E_∞ is associated with the width of the distribution of correlation times: the larger the distribution, the smaller the value of E_∞, for the same mean correlation time. Figure 5a shows the 2D exchange spectrum of the same sample at −75 °C. The observed decrease in the number of contour lines indicates the expected decrease in the number of segments executing large-angle reorientations. This is confirmed in the $E(t_m, \delta\tau_{CSA})$ versus $2\tau_{CSA}$ curve shown in Figure 5d, which can be simulated using the same model, but with a smaller fraction of segments executing isotropic reorientations. The small final value of the $E(t_m,\delta\tau_{CSA})$ curves, ~0.15, indicates that about 85% of the polymer segments are moving out of the milliseconds to seconds time scale at −75 °C.

Once the motional behavior of the $[88]_{45}$-II sample is characterized, it is important to investigate the effect of the polymer chain length on the slow dynamics of the ormolytes. To achieve this goal, the same kind of experiments were performed for the sample $[66]_{11}$-II. Despite the difference in the polymer percentage, which is a consequence of the sample preparation, these measurements can give some insight into the motional behavior of the polymer in the hybrids. Parts (a)−(c) of Figure 6 show the 2D exchange spectra obtained for the sample with very short polymer chain length $[66]_{11}$-II

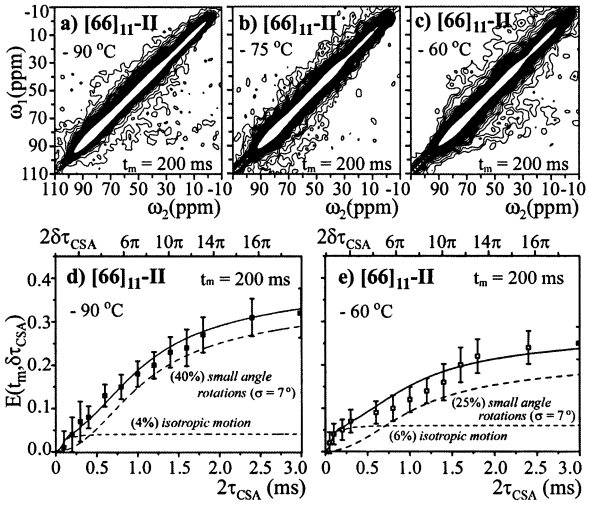

Figure 6. Results of exchange experiments performed for the $[66]_{11}$-II hybrid. (a), (b), and (c) 2D exchange spectra at −90, −75, and −60 °C. (d) Pure exchange intensity $E(t_m,\delta\tau_{CSA})$ versus $2\tau_{CSA}$ at −90 °C. (e) Same as in (d) at −60 °C. The simulations were carried out using the same procedures used in Figure 5. The contour levels were taken from 5 to 20% of the maximum height.

at −90, −75, and −60 °C. As the transition from the intermediate to the slow motion regime is not well-defined for this sample, Figure 3i, the measurements were performed in these three temperatures. The observed 2D spectra are very similar at −90, −75, and −60 °C, indicating the predominance of small-angle motions. This is confirmed in the $E(t_m,\delta\tau_{CSA})$ versus τ_{CSA} curves at −90 and −60 °C shown in (d) and (e) of Figure 6. The low off-diagonal intensity in the 2D exchange spectra and the predominance of small-angle contribution in 1D PUREX curves indicate that the covalent bonding hinders the slow molecular motion of most polymer segments in $[66]_{11}$-II ormolytes. However, the $[CH_2CH_2O]_n$ line observed at 20 °C indicates the presence of isotropic rotations in the fast motion limit. Then, it can be supposed that in this case the transition from slow to fast motion involves both a decrease in the correlation time and an increase in the fraction of molecular segments executing large-angle motions. This hypothesis is corroborated by the initial increase of the $E(t_m,\delta\tau_{CSA})$ versus $2\tau_{CSA}$ curve, which are possibly associated with a little fraction of the segments executing isotropic reorientations, Figure 6d. At higher temperatures this small fraction probably increases until most of the chains execute fast isotropic motions. Furthermore, the broader lines in the spectrum of sample $[66]_{11}$-II at 20 °C, shown in Figure 3d, indicate that the molecular motion of the groups close to the linkage is hindered even at this temperature. Taking all these statements together, it can be concluded that in Type II ormolytes the hindrance of the molecular motion increases with the proximity of the linking group, as already observed in ref 7.

Figure 7 shows the 2D exchange spectra and the 1D PUREX curves for the nonbonded ormolytes. An intense off-diagonal pattern is observed in the spectrum of the sample $[50]_{45}$-I at −60 °C, Figure 7b, revealing the presence of large-angle reorientations. These large-angle motions also show up in the respective 1D PUREX curve shown in Figure 7d. A decrease in the off-diagonal

(36) Saalwächter, K.; Schmidt-Rohr, K. *J. Magn. Reson.* **2000**, *145*, 161−172.
(37) Harris, D. J.; Bonagamba, T. J.; Schmidt-Rohr, K. *Macromolecules* **1999**, *32*, 6718−6724.
(38) Schaefer, D.; Spiess, H. W. *J. Chem. Phys.* **1992**, *97*, 7944−7954.

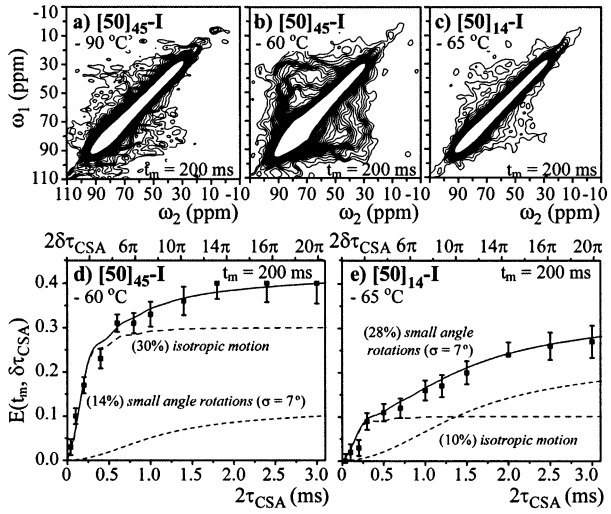

Figure 7. Results of exchange experiments performed in the Type I ormolytes. (a) 2D exchange spectrum at −90 °C for the $[50]_{45}$-I hybrid. (b) Same as in (a) at −60 °C. Large amplitude reorientations are clearly observed in this spectrum. (c) 2D exchange spectrum at −65 °C for the $[50]_{14}$-I hybrid. (d) Pure exchange intensity $E(t_m,\delta\tau_{CSA})$ versus $2\tau_{CSA}$ for the $[50]_{45}$-I hybrid at −60 °C. (e) Pure exchange intensity $E(t_m,\delta\tau_{CSA})$ versus $2\tau_{CSA}$ for the $[50]_{14}$-I hybrid at −65 °C. The simulations were carried out using the same procedures used in Figure 5. The contour levels were taken from 5 to 20% of the maximum height.

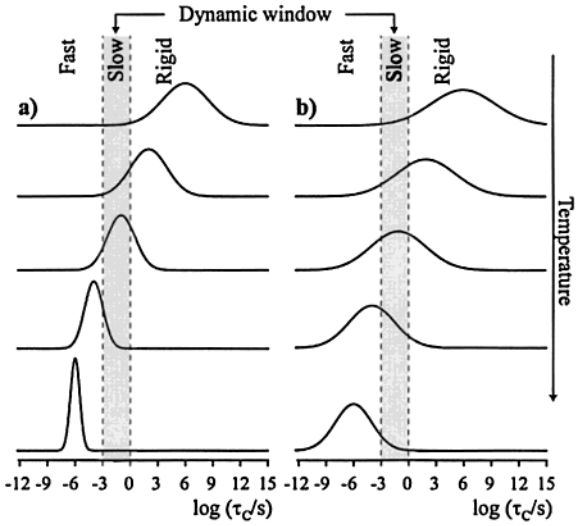

Figure 8. Pictorial view of the sharpening of a log-Gaussian[38] distribution of correlation times as a function of temperature. A rough representation of the motional regimes is shown. In (a) the fraction of slow-moving segments (shaded portion of the Gaussian function) varies with temperature. In (b) a broader distribution of correlation times with slower sharpening as a function of temperature produces less variation in the fraction of slow-moving segments. As the motional narrowing starts when some segments achieve the intermediate motional regime, a slower slow to fast transition is expected in case (b).

intensity is observed at −90 °C, Figure 7a, indicating the slow down of the molecular motion (compare (a) and (b) in Figure 7). A significant diagonal contribution is also observed in these spectra, indicating that a portion of the segments moves out of the milliseconds to seconds time scale or executes small-angle rotations. This is confirmed in the $E(t_m,\delta\tau_{CSA})$ versus t_m curves shown in Figure 7d, where a fraction of small-angle rotations is used in the simulations. It is well-known that, even for nonbonded ormolytes, the mobility of the polymer segments is affected by the interaction with the silica clusters. For this reason, the lower exchange intensity found for the sample with shorter polymer chain $[50]_{14}$-I, Figure 7c,e, may indicate that the interaction with the silica structure is more effective in this case, producing a higher hindrance to the molecular motion. However, because the mobile fraction varies with temperature, it is not possible to confirm this statement only with the results presented in this work.

Additional discussion can be done if one compares the motional behavior of bonded and nonbonded ormolytes with similar chain lengths. For the experiments carried out at temperatures where the correlation times for all the samples are similar, Figure 4, the percentage of polymer segments executing "free" isotropic rotations is smaller in bonded than in nonbonded samples (see Figures 5−7). This suggests that the nature of the chemical bonds plays an important role in the dynamics of the polymer in these hybrid materials, being more pronounced for very short chains.

Distribution of Correlation Times. Alternatively, the motional heterogeneities can be discussed in terms of distribution of correlation times. The appearance of large-angle contribution in the 2D exchange spectrum would depend on having a considerable number of segments executing these motions in the milliseconds to seconds time scale; that is, the width of the distribution of correlation times must be sharp enough (smaller than 3 decades) to fulfill this condition. On the other hand, Spiess et al.[18] have shown that the width of the distribution of correlation times varies with temperature during the polymer glass transition. It was shown that the width of the distribution of correlation times increases with a decrease in temperature accompanied by an increase in the mean correlation time of the molecular motion. Therefore, the detection of large-angle reorientations in the exchange experiments depends on the distribution of correlation times and on its sharpening as a function of temperature. Following this idea, a broader distribution of correlation times and a slower narrowing of this distribution with the temperature would be in agreement with the absence of significant large-angle contribution to the exchange intensity of sample $[66]_{11}$-II. Furthermore, at temperatures above −60 °C, the tail of the distribution of correlation times starts producing the motional averaging of the line shape and, at 20 °C, the distribution becomes sharp enough to have all the molecular segments executing large-angle motions in the fast motion regime; that is, sharp lines are observed. Figure 8a shows a pictorial view of the above discussion. For the sample $[88]_{45}$-II, large-angle motions are observed in the 2D exchange spectrum; consequently, narrower distributions of correlation times in the slow motion regime and faster sharpening of these distributions as the fast motion regime approaches is expected, Figure 8a. In the case of a broader distribution of correlation times, Figure 8b, a slower transition from slow to fast motions would be expected. Hence, the slower motional narrowing observed for sample $[66]_{11}$-II in Figure 3i is also an indication of a broader distribution of correlation times, that is, a higher degree of motional heterogeneity.

Conclusions

The slow dynamics of siloxane/poly(ethylene glycol) hybrid materials was studied using 1D and 2D static exchange NMR experiments. For Type II ormolytes, where the poly(ethylene glycol) chains are covalently bonded to silica structures, it was shown directly from the 2D exchange spectra that in the slow motion regime the motions of the polymer segments near the linkage group are restricted and do not execute large amplitude motions. In addition, it was demonstrated that the molecular motion in bonded ormolytes is more hindered for samples with smaller chain length, whose spectra do not show considerable exchange intensity in the slow motion regime. This distinct behavior is attributed to differences in the dynamic heterogeneities of the molecular motion in the two samples. Similar results are found for nonbonded ormolytes, but in this case the dynamic heterogeneities are less pronounced than those in the case of the bonded hybrids. Therefore, the results revealed that the heterogeneities of the slow molecular motions of the polymer chains depend on the chain length and the nature of the interaction between the organic and inorganic phases. Further measurements on Li^+-doped ormolytes are in progress to correlate these results with the ionic mobility.

Acknowledgment. The Brazilian agencies FAPESP, CNPq, and Brazil-France project USP-COFECUB supported this research. D.R. thanks the Deutsche Forschungsgemeinschaft DFG for financial support.

CM020947V